Shock Waves (2024) 34:399–412
https://doi.org/10.1007/s00193-024-01167-4

ORIGINAL ARTICLE

Investigation into helmet–head shock wave interactions at low overpressures through free-field blasts and schlieren imagery

C. J. H. Thomas[1] · C. E. Johnson[1]

Received: 13 March 2023 / Revised: 4 March 2024 / Accepted: 21 March 2024 / Published online: 22 May 2024

Abstract

Brain injuries in warfighters due to low-level blasts, even while wearing a helmet, are common. Understanding how the form of a shock wave changes when impacting a head donning a helmet may present solutions to reducing shock loading on the head, thereby reducing the prevalence of blast-induced traumatic brain injury. A manikin with PCB piezoelectric transducers throughout the head was exposed to low-pressure free-field blasts using an RDX-based explosive charge designed to output a side-on overpressure of 4 pounds per square inch (psi) [27.5 kilopascals (kPa)] with and without a helmet. Orientations of 0, 45, 90, 135, and 180 degrees were evaluated to observe changes in overpressure versus time ($p(t)$) waveforms. The waveforms were compared to schlieren imagery in which a shock wave impacted 3D-printed silhouettes of a warfighter donning a helmet, showing shock wave flow under the helmet at 0-, 90-, and 180-degree orientations. It was found that trapped shock waves under the helmet create regions of high overpressure and increase the duration of exposure, resulting in higher impulses imparted onto the head. While wearing a helmet, the 90-degree orientation resulted in the greatest reduction in overall peak overpressure, with an 8% decrease compared to the 0-degree orientation. In contrast, the 180-degree orientation led to an increase by 30%. For impulse, the 90-degree orientation showed the greatest reduction, with a decrease of 21%. The 0-degree orientation had the highest overall impulse among all orientations when wearing a helmet.

Keywords Blast-induced traumatic brain injury (bTBI) · Schlieren imagery · Underwash effect

1 Introduction

Ensuring warfighters stay within a safe blast exposure limit, both during training and on the battlefield, has proven challenging [1]. The definition of safe exposure limits is pivotal to understanding this issue. Researchers have attempted to establish definitive blast exposure limits, aiming to achieve consensus in this regard. A pivotal step toward this objective has been taken through a definitional study [2]. In this study, blast events ranging from 74.5 kilopascals (kPa) (10.8 pounds per square inch (psi)) to 116.7 kPa (16.8 psi) were categorized as low-to-moderate-level blasts. In the same study, blast events > 100 kPa (14.5 psi) were identified as moderate-to-high intensity blasts for chronic exposures. Thus, until definitions have been adopted widely by researchers, it is imperative to define "low-level" exposure in blast studies. For clarity in this discussion, exposures below 74.5 kPa will be classified as "low-level," but not as "safe." Historically, the established threshold for safe blast exposure was 4 psi (27.5 kPa), as reflected in army doctrine manuals citing 3.4 psi (23.4 kPa) as an exposure with a 1% chance of eardrum rupture [3]. However, recent research involving mice subjected to repeated low-level blasts resulted in blast-induced traumatic brain injuries (bTBI) [4], accompanied by symptoms of depression and anxiety, in the mice exposed to shock tube tests replicating such blasts [5]. In the field, breachers also encounter mild forms of bTBI, colloquially referred to as "breacher's brain" [6]. In response to this issue, researchers are actively working to understand the nature of this problem and how helmets can help protect the wearer.

Advances in helmet design have allowed users to be protected against ballistic threats such as shell fragments or bullets [7]; however, helmet protection has yet to make as

Communicated by R. Banton, T. Piehler, R. Shoge.

✉ C. E. Johnson
Catherine.Johnson@mst.edu

C. J. H. Thomas
codythomas@mst.edu

[1] Mining and Explosives Engineering, Missouri University of Science and Technology, 290 McNutt Hall, Rolla, MO 65409, USA

much progress in protection against shock waves that can result in bTBI [8, 9]. Although there are different possible mechanisms causing bTBI, the main four mechanisms proposed thus far are direct transmission, skull deformation, head acceleration, and thoracic compression [10]. Direct transmission is when the stresses caused by the shock waves are transmitted through the material of the head into the brain and foramina [11]. Skull deformation occurs when high-rate loading on the skull structure induces localized flexure. Head acceleration causes brain damage by either decoupling of the brain and skull motion or indirect inertial forces. Thoracic compression is thought to be caused by the compression of the chest leading to a high vascular surge to the brain. Of those proposed mechanisms, proper helmet design can potentially limit the damage done by skull deformation and direct transmission by limiting shock wave loading onto the wearer's head.

As a shock wave interacts with a head while a helmet is worn, the wave has been shown to get trapped under the helmet, causing reflections between the head and the helmet due to the acoustic impedance mismatch of the air in which the wave is traveling, and of that of the skull and the helmet [12]. In addition to this mismatch, it is understood that the initial overpressure is amplified by the reflection off a surface, which has a higher impedance than the air [13, 14]. Therefore, it is expected that when a shock wave is confined underneath the helmet, the overpressures would be sustained over a larger area of the head in contrast to a helmet not being worn. Additionally, shock waves trapped underneath the helmet collide, increasing the overpressure magnitude, known as the underwash effect [15, 16]. Both effects result in larger overpressures under the helmet, and many researchers have found that the presence of a helmet will lead to higher overpressures experienced on the head [10, 15, 17–20]. Several different methods have been proposed to reduce the underwash effect. One method that has been suggested involves using foam pads that fit tightly [20] or incorporating complex geometric passages to diffuse shock waves under the helmet [21]. Another approach is to modify the suspension pads using a shear-thickening fluid or polyurea [22] to dampen the shock wave. These promising solutions are still under study, and the underwash effect is still being observed in more recent free-field [16] and shock tube [17] tests.

Current research into the helmet protection related to bTBI has been a combination of computational modeling, shock tube, and free-field blast studies. Most recent studies have been either shock tube or computational modeling. A summary of the computational studies on the subject gathered by Skotak et al. [23] is updated in Table 1 to include the surrogate human head shock tube and free-field blast studies with and without a helmet. Of the three methods, free-field blast testing creates an open-field explosive blast wave similar to simple Friedlander waves, which mimic clinical cases where blast exposure occurs in an open area with no obstacles to impede the blast wave expansion. However, due to the complexity of setting up free-field blasts, few free-field blast studies examine shock wave head interactions, as shown in Table 1. Previous free-field studies mimic a blast exposure produced by an improvised explosive device (IED) instead of exposure levels that could be experienced in training or breaching. Although IEDs can be in a range of sizes, with vehicle-based IEDs being quite large, a recent computational study used the example which resulted in an overpressure of 6000 mm of mercury (mmHg) (116 psi/800 kPa) as an example of an IED blast [24]. The blast orientations found in the literature search included frontal (0-degree), side (90-degree), and rear blasts (180-degree), with the majority being 0-degree.

This paper presents a free-field experimental comparison of an instrumented manikin head with and without a kevlar-based helmet exposed to low-level blasts by an RDX-based explosive. These free-field blasts provide baseline overpressure and impulse values for the military overpressure exposure of 27.5 kPa (4 psi). Additionally, 3D-printed silhouettes of the cross sections of a warfighter wearing a helmet were filmed at high speed using a schlieren imaging technique to visualize the shock wave flow under the helmet. Comparing results from these two methods gives possible explanations for the resulting overpressures under the helmet due to shock wave interactions. Free-field blast studies are sparse, and this is one of the first free-field blast studies examining low-level blasts for a range of orientations using an anatomical model, which allowed the role the torso and shoulder reflections play in increasing overpressure under helmets to be fully examined.

2 Methodology

Both schlieren imaging and free-field blasts were used to investigate shock wave flow and loading on a manikin head. Free-field blasts allowed for different parts of the head to be evaluated for overpressure, impulse, duration, and rise time. These measurements were compared to the fluid motion seen underneath a 2D cross section of a helmet in schlieren imaging to understand how shock wave flow relates to the results obtained in the free-field blasts.

2.1 Free-field experimental method

The helmet was tested using a modified manikin constructed from the torso and head of a manikin model MM-BC8S [41], representing a 5-ft 8-in (173-cm) fleshtone male, with the following modifications. Holes were drilled into the head, and metal threads were epoxied on the inside, allowing PCB Piezotronics Model 102B18 and 102B15 high-frequency ICP

Table 1 A summary of free-field, shock tube, and computational modeling tests on surrogate human head models conducted to evaluate helmet performance

References	Type	Orientations	Tested overpressure (kPa)	Tested overpressure (psi)
Li et al. [16]	Free-field, computational model	0, 90, 180	260, 290[b]	37.7, 42.1
Mott et al. [15]	Free-field	0, 45, 90, 180	195[b]	28.3
Downe et al. [18]	Free-field[a], computational model	0	198.9	28.8
Chandra et al. [19]	Free-field, shock tube	0	264.4[a]	38.3
Ouellet and Philippens [10]	Free-field, shock tube	0	137.9	20.0
Azar et al. [17]	Free-field	0	86.1	12.2
Skotak et al. [23]	Shock tube	0, 90, 180, 270	35, 70	5.1
Ganpule et al. [20]	Shock tube	0	180	26.1
Ganpule et al. [25]	Shock tube	0	70, 140, 200	10.2
Hosseini-Farid et al. [26]	Computational model	0, 90, 180	55, 230, 450[b]	7.98, 33.4, 65.3
Mott et al. [27]	Computational model	0, 90, 180	120	17.4
Zhang et al. [28]	Computational model	0, 90, 180	270–660	39.2–95.7
Tan et al. [29]	Computational model	0	103	14.9
Zhang et al. [30]	Computational model	0	180	26.1
Jazi et al. [31]	Computational model	Overhead	407	59.03
Sarvghad-Moghaddam et al. [32]	Computational model	0, 90, 180	450	65.3
Sarvghad-Moghaddam et al. [33]	Computational model	0, 90, 180	520	75.4
Singh and Cronin [34]	Computational model	0	170, 326	24.7, 47.3
Sarvghad-Moghaddam et al. [35]	Computational model	Over/under head, 0, 180	520	75.4
Sharma [36]	Computational model	0, 90	70, 150	10.2, 21.8
Grujicic et al. [37]	Computational model	0	520, 1886	75.4, 273.5
Makris et al. [38]	Computational model	0	441.4[b]	64
Tan and Bagchi [39]	Computational model	0, 90, 180	103.4	15
Yu and Ghajari [40]	Computational model	0, 90, 180	200, 300, 500	29.0, 43.5, 72.5

This table has been adapted from Table 2 in a study by Skotak et al. [23]; the studies not directly testing helmets were removed

[a]Free-field test where head was studied but no helmet

[b]Calculated using Kingery–Bulmash equations

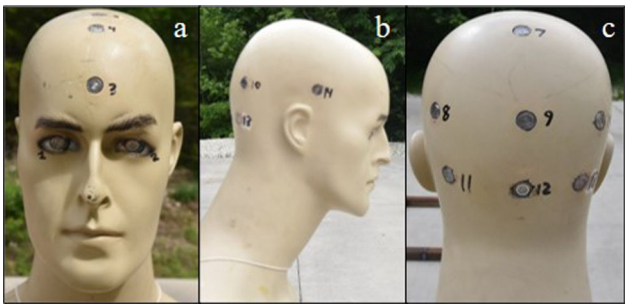

Fig. 1 **a** The sensor locations on the front of the head, **b** side of the head sensor locations, **c** back of the head sensor locations. Sensors 14 and 15 are in line with one another, with sensor 15 on the left side of the head

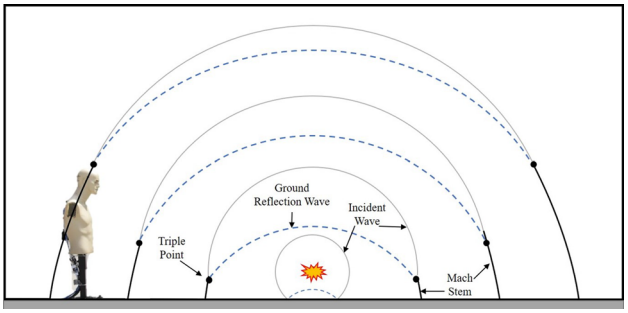

Fig. 2 Diagram of a free air burst expansion. The incident wave is the solid gray line, reflected wave is the blue dotted wave, and the Mach stem is the solid black line

sensors to be mounted flush with the exterior of the head [42]. The sensor wires were let out the back for connection to a Synergy Hi Techniques data acquisition system (DAS) [43]. The manikin was then filled with Clear Ballistics' ballistic gel [44] to eliminate the void inside the manikin and dampen vibrations, which could cause noise in the data. The torso was mounted onto a metal stand that could be bolted to the ground and rotated in orientations of 0, 45, 90, 135, and 180 degrees from the blast source. The locations for the sensors are shown in Fig. 1. Sensors 1 and 2 are in the eye sockets and will be referred to as the right and left eye. Sensors 3 to 5 move back along the frontal midline of the head, with 3 being the forehead. Sensor 6 is the highest point of the skull or vertex of the head. Sensors 7 to 10 are along the midline of the parietal with 8 and 10 on the left and right, respectively. Sensors 11 to 13 move left to right on the occipital, or lower back section, of the head. Sensors 14 and 15 are on the temporal, or side, part of the head, on the right and left, respectively.

Sensors directly facing the blast were expected to receive a head-on overpressure from a normal wave reflection, while sensors on top and side of the head would receive side-on overpressure. With the presence of a helmet, sensors covered by the helmet would receive an overpressure resulting from one or more, typically oblique, wave reflections. During testing with the helmet, chin straps were securely tightened onto the manikin's chin to provide realistic coverage of the head and contact of foam pads with the head.

During a suspended air blast, an incident wave is created, which reflects off the ground creating a ground reflected wave. In the event these two waves interact individually with the manikin, the two waves will complicate the waveform profile compared to a single blast wave with Friedlander characteristics of a fast rise time and single exponential decay. The incident shock reflection from the ground is initially of regular type, with subsequent transition to Mach reflection and formation of a Mach stem. The point where the Mach stem, incident, and reflected waves intersect is known as the triple point. This interaction is shown in Fig. 2.

To ensure this uniform Mach stem wave under the triple point interacts with the manikin, the figures from UFC-340-02 [45], which relied on data from Swisdak [46], were used to determine the height of the charge to produce triple points which would be above the manikin, resulting in a single blast wave interaction. Data from these sources also allowed the distance and charge size to be chosen for a predicted 27.5 kPa (4 psi) side-on overpressure wave at the top midline of the head (sensor 5). The 27.5 kPa (4 psi) overpressure was chosen as it is the safety standard threshold for the U.S. Army. This overpressure equates to 41 g of the RDX-based explosive at a distance of 2.5 m and a height of 0.3 m, as shown in Fig. 3. With this placement of the charge, it ensured that the manikin was under the triple point, in the Mach stem location.

Another consideration during explosive testing is the inherent variance due to factors such as atmospheric conditions, material aging, and charge density, all of which affect explosive performance. In order to assess the consistency of the RDX-based explosive used in this study, three trials with a 135-g charge size at a 2.5-m distance in the 0-degree orientation were conducted to simulate 82.7 kPa (12 psi). Tests were performed without a helmet, and peak pressures were collected to analyze variance, shown in Fig. 1 in the Supplementary Information. Results indicate higher scatter in sensors closest to the blast. Sensors closer to the blast in this orientation measure a reflected component as their angle in relation to the blast is between 0 and 90 degrees. Piezoelectric pressure sensors in the side-on orientation, 90-degree, will receive side-on pressure for a long duration, making measurement readings possible even with lower sample rate data acquisition systems. On the other hand, sensors facing the blast will receive a total reflected pressure, which lasts only for a very short duration, leading to higher scatter in the data. As the orientation of the head will change between tests, sensors with more or less of the scatter will also change between tests, so that analyzing scatter for a specific sensor would not

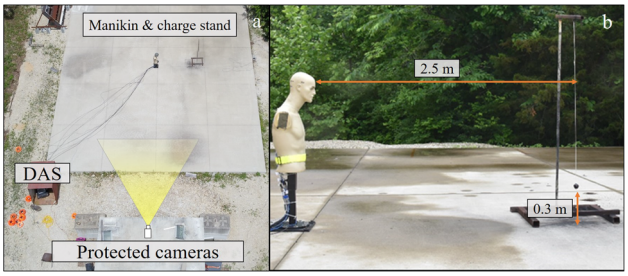

Fig. 3 **a** The overhead setup of the free-field blast. **b** A 41-g explosive charge suspended at a height of 0.3 m and a distance of 2.5 m away from the manikin with the helmet not worn. This combination of charge size, distance, and height creates a uniform Mach stem to impact the manikin

be applicable. Therefore, the analysis will be between the angles for helmet and no helmet data. The objective of this study was to evaluate the effects of warfighter's orientation when exposed to blast loads rather than loading consistency. With this in mind, the reader should note while reading the analysis that one repeat of each trial was performed during this study.

The coaxial cables from the manikin were connected to the DAS, which was placed in a protective shelter nearby, as shown in Fig. 3a. To document the blast, a monochrome Phantom V2012 high-speed camera [47] recording at 100,000 frames per second (fps) was used. For these tests, the manikin stand was rotated to allow the manikin to experience a blast from 0-, 45-, 90-, 135-, and 180-degree orientations, where Fig. 3b shows the 0-degree, head-on orientation. A single test at each orientation was conducted for a total of 150 waveforms analyzed. While it is known that air blast test results can vary due to changes in the explosive size, geometry, and density, efforts were taken to minimize variance in these factors by using 3D-printed charge molds for uniform geometry, mass, and density for each test. Distance was controlled by fixing the manikin stand to the concrete blast pad with charge distance measured with a tape measure with 1-mm divisions.

2.2 Schlieren experimental design

Schlieren imaging was used to observe a shock wave moving throughout the cavity between the helmet and head to visualize part of the underwash effect. Two cross sections of a warfighter wearing the helmet were created from a graphic training aid on the proper wearing of the helmet for evaluation in the 0-, 90-, and 180-degree orientations. The 2D cross section view in Fig. 4 shows the area beneath the helmet with no helmet pads, enabling observation of wave movement. These cross sections were 3D-printed, Fig. 4a, placed into a schlieren setup, shown in Fig. 4b, and exposed to shock waves produced by NONEL DYNO lead line [48]. The cross

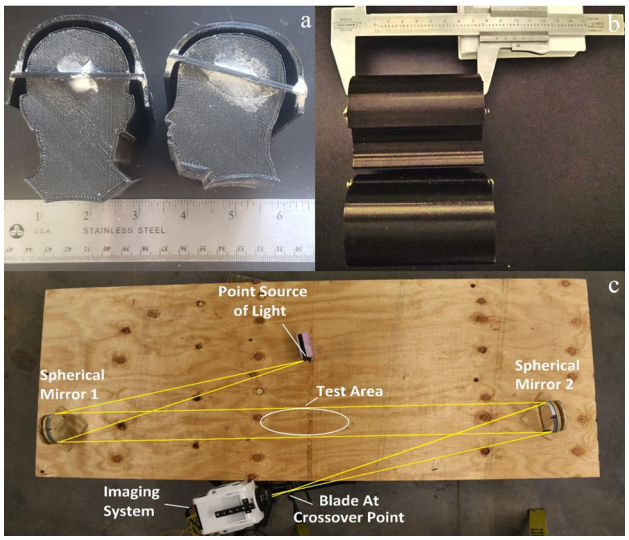

Fig. 4 3D-printed cross sections: front views at 0 and 90 degrees (**a**), the side views of the same pieces (**b**), placed in the schlieren test setup (**c**) for analysis

sections were 85 mm long to limit the shock wave wrapping around the cross sections, with the thickness of the helmets between 2.5 and 3 mm, and the gap between the helmet and head being 2 to 7 mm. The wave–helmet interactions were filmed with a monochrome Phantom V2012 high-speed camera at 100,000 fps. A Z-style schlieren setup was used with two confocal mirrors set at a distance of two focal lengths with a point light source and test area directly between them. A blade was used at the cross-over point to emphasize the shock front.

3 Results and analysis

3.1 Free-field blasts

Peak overpressure and impulse experienced on the head are important factors in assessing how a shock wave causes skull deformation and direct transmission [49]. The shock waveforms shown in Fig. 5 are for the 0-degree front blast with and without the helmet. While this analysis will primarily focus on waveforms from three sensors, waveform data from all 15 sensors can be found in the Supplementary Information. Without the helmet, the head experiences a traditional Friedlander waveform, with fast rise times of less than 0.10 ms shown in the forehead sensor (sensor 3) and vertex sensor (sensor 6) before a slow decay of pressure (Fig. 5a). A shock wave reflection from the shoulders moves up toward the head resulting in the slower rise time of 0.29 ms and non-traditional waveform on the lower back of the head (sensor 12). Although the decay rate was slower than for the forehead and vertex sensors, all three decays had a similar shape.

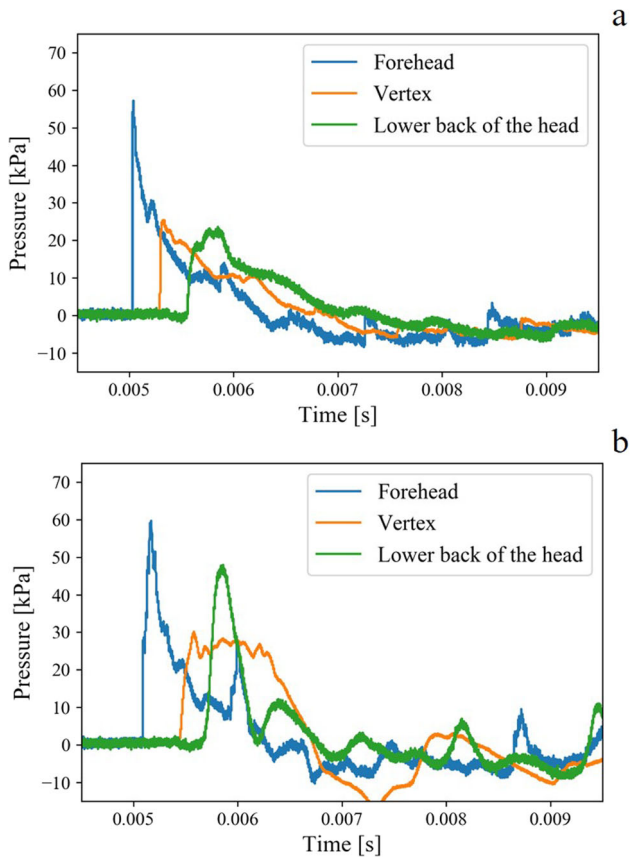

Fig. 5 **a** The 0-degree waveform on forehead, vertex, and lower back of the head sensors when not wearing a helmet. **b** The same sensors but with the addition of the helmet

The overpressure at the vertex sensor is 25.4 kPa, close to the designed overpressure of 27.5 kPa in the side-on orientation. Overpressure at the forehead is higher at 57.2 kPa, a 70.1% difference. It should be noted that this is expected as the location was slightly closer to the blast source in addition to the orientation where the overpressure was caused by an oblique wave reflection.

When a helmet is added, the predictable nature of the waveforms is changed. The wave experienced on the vertex sensor, shown in Fig. 5b, is a notable example of this waveform change. These waveform changes include a peak overpressure increase of 17%, rise time increase by 106%, and duration of the wave decrease by 33%. The waveform duration is extended at higher pressure resulting in an impulse increase of 54% when the helmet is added. These waveform changes have been previously described as the pressure rising in stages, rather than a fast rise time, where a shock wave would impart a lot of its energy all at once. This difference in rise of pressure is likely due to the diffraction and reflection of the shock wave moving under the helmet [16], which results in the buildup of pressure in the affected area under the helmet. This, in turn, creates areas of high overpressure under the helmet on the back of the head due to collisions imparting an increase in overpressure and impulse on the lower back of the head. These areas of overpressure indicate that the underwash effect was observed. The lower back of the head sensor's peak overpressure increased by 68%, rise time decreased by 52%, duration decreased by 55%, and impulse increased by 2% when a helmet was added. In this 0-degree orientation, the head overall experienced a 26% increase in peak overpressure, 74% increase in rise time, 28% decrease in positive phase duration on the head, and a 24% increase in impulse when a helmet was added. These important values are presented in Table 2, along with percentage difference between values collected. The most significant percentage differences indicate areas where the inclusion of the helmet has led to notable changes in shock wave values and also help identify which sensor was most influenced. Despite conducting a single test with and without the helmet for each orientation in this study, it is essential to examine the data in Table 2 and refer to Fig. 1 in the Supplementary Information, which illustrates a three-repeat test example without a helmet. This comparison helps contextualize the conclusions drawn from the study. Notably, the 0-degree data in Fig. 1 (Supplementary Information) indicate that the highest scatter between tests would be expected on the forehead. However, the study's data comparing a helmet to no helmet situation in the 0-degree orientation reveal the greatest difference at the back of the head. This suggests that the observed difference is likely attributable to the presence of the helmet rather than testing scatter. In future studies, additional repeats are recommended to confirm exact percentage difference. Complete breakdowns of impulse and peak overpressure change due to the presence of the helmet are shown in the Supplementary Information.

One of the largest percentage differences in Table 2 is the difference in rise time on the forehead sensor. Further inspection of the waveforms on the forehead sensor can be seen in Fig. 6c. Comparing the waveforms of the pressure wave with and without the helmet, both initially have sharp overpressure rises. However, as the wave reflects between the head and the helmet, the waveform is changed, and reflections create an area of high pressure for longer than the wave was able to impact the forehead and reflect off. This results in the peak overpressure occurring a short time after the initial rise resulting in a longer rise time, shown by the large percentage difference of 155%.

In addition, examination of the waveforms on the forehead shows a noticeable secondary spike in the data at a similar time with or without the helmet, as seen in Fig. 6c. This is most likely caused by the reflection of a wave off the shoulder and up toward the forehead sensor. When the helmet is worn, the wave gets trapped under the helmet, allowing for multiple reflections and preventing a gradual decay in overpressure, whereas when the helmet is not worn, there is an

Table 2 0-degree orientation peak overpressure, rise time, positive phase duration, and impulse values for forehead sensor (3), vertex (6), and lower back of the head (12), presented for both helmet (H) and without helmet (NH) scenarios, along with the percentage difference between the two experimental values

0-degree orientation	Forehead			Vertex			Lower back head		
NH/H	NH	H	Diff.%	NH	H	Diff. %	NH	H	Diff. %
Peak overpressure (kPa)	57.2	59.9	4	25.5	30.3	17	23.4	47.6	68
Rise time (ms)	0.01	0.08	155	0.04	0.13	105	0.3	0.2	52
Positive phase duration (ms)	1.3	1.3	6	1.9	1.3	33	2.1	1.2	55
Incident impulse (kPa·ms)	18.6	21.4	16	15.2	26.2	54	15.9	16.5	2

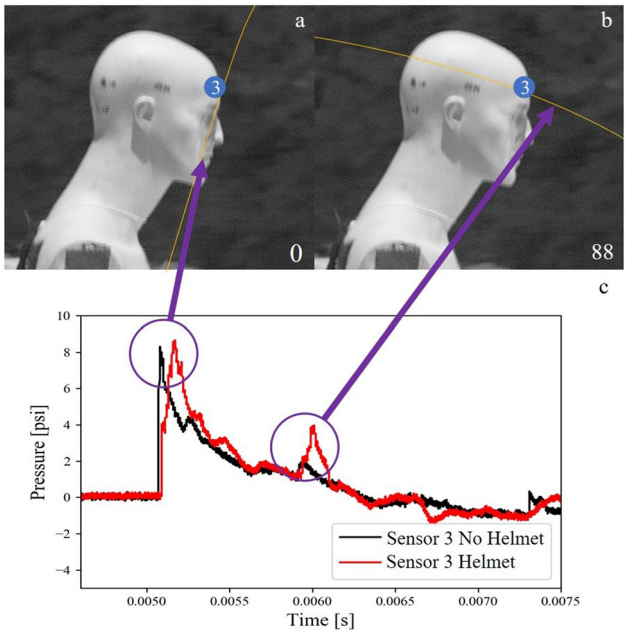

Fig. 6 **a** The high-speed footage frame at which the shock wave initially reaches the forehead and **b** the frame at which the shock wave's reflected wave reaches forehead, 88 frames later. **c** Comparison of the forehead data with and without the helmet in the 0-degree orientation

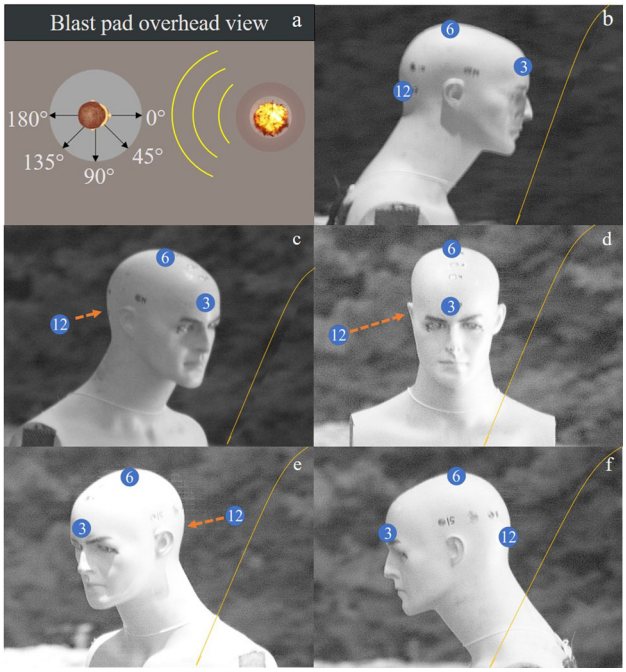

Fig. 7 **a** Manikin orientation for all tests conducted, where the manikin was rotated relatively to the blast source. The shock wave (yellow line) approaches the following orientations: **b** 0-degree, **c** 45-degree, **d** 90-degree, **e** 135-degree, and **f** 180-degree

overpressure rise and then gradual decay. Further analysis of high-speed footage confirms the occurrence of the wave reflection off the shoulders with initial impact at the forehead sensor at 0 frame, and 88 frames later, the reflected wave is seen moving past the forehead sensor seen in Fig. 6b. When the helmet is worn, the inner part of the reflected wave is seen moving into the helmet with the outer part of the wave moving past the helmet 85 frames later. The high-speed footage captured in this study at a frame rate of 100,000 fps enabled the observation of the shock wave impact, the initial spike, and the reflected wave moving up into the forehead sensor, where the secondary spike occurs approximately 0.85 ms after the first spike as depicted in Fig. 6c. High-speed imaging of each manikin orientation, shown in Fig. 7, allowed for a closer understanding of the shock waveforms.

Figure 8 shows overpressure waveforms for the 45-degree orientation for the forehead, vertex, and lower back of the head sensors. When the user's orientation changes from 0-degree to 45-degree, the waveform on the lower back of the head (sensor 12) follows the Friedlander shape more closely because the wave impacts the shoulder differently, causing the shock wave to reach the back of the head faster (Fig. 8a). When a helmet is added, the overpressure spike on the lower back of the head is less pronounced. As the wave reaches the top of the head, a higher impulse occurs due to the helmet trapping the wave, but the peak overpressure is not as high as that experienced during a front blast. When a helmet was added in this orientation, the head overall experienced a 16% increase in peak overpressure, 129% increase in rise time, 28% decrease in duration, and 14% increase in impulse.

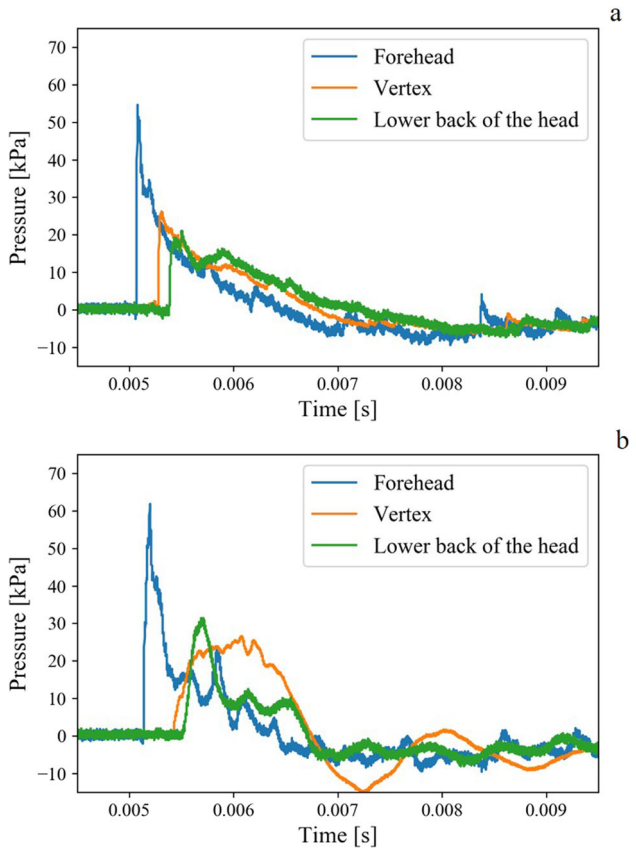

Fig. 8 **a** The 45-degree waveforms on the forehead, vertex, and lower back of the head sensors when not wearing a helmet. **b** The same sensors but with the addition of the helmet

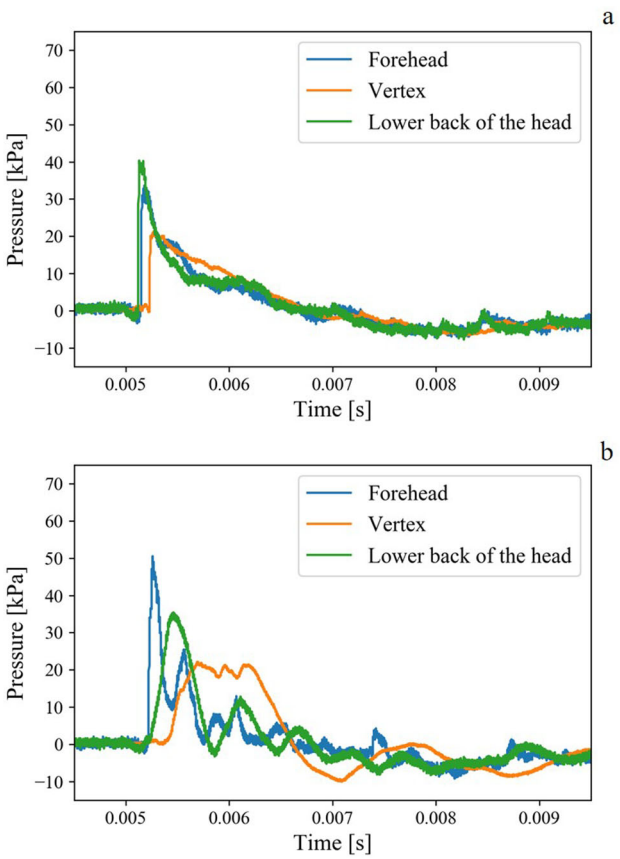

Fig. 9 **a** The 90-degree waveforms of the forehead, vertex, and lower back of the head sensors when not wearing a helmet. **b** The same sensors but with the addition of the helmet

When the manikin is subjected to a 90-degree blast (Fig. 9), the shock wave arrives at the forehead and back of the head sensors nearly simultaneously. Shortly after that, the shock wave moves up and impacts the top of the head (sensor 6). This can be seen by the time of arrival for the forehead sensor and lower back head sensor happening before the top sensor in Fig. 9a. The waveform decays on the back and front of the head are also nearly identical. After a helmet is added, these waveform decays are changed as the movement of the shock wave is trapped under the helmet, causing overpressure spikes. In this orientation, when a helmet was added, the head experienced a 14% increase in peak overpressure, 45% increase in rise time, 44% decrease in duration on the head, and a 1% decrease in impulse. Another contributing factor to the change in waveforms in this orientation is that more of the head is protected from a direct impact from the shock wave. Lastly, observations included the reflected wave from the shoulder closest to the blast entering under the helmet and resulting in a secondary spike, at approximately 5.5 ms, in overpressure on the forehead (Fig. 9b). During that time, the lower back of the head also experiences wave decay.

When the shock wave impacts the manikin during a 135-degree blast, waveform decay resembles normal Friedlander decay. However, the neck appears to change the impact on the back of the head, causing an abnormal rise time on the lower back of the head (Fig. 10a). On the forehead sensor (Fig. 10a), a reflection off the shoulder results in a secondary spike in overpressure. The angle of the shock wave approach and the helmet appear to change the impact of the shock wave to the top of the head, with the secondary spike seen. In this orientation, when a helmet was added, the head overall experienced a 30% increase in peak overpressure, 6% increase in rise time, 23% decrease in duration on the head, and 7% increase in impulse.

During a 180-degree blast, the back of the head receives a large overpressure increase, but the front does not receive as large of an increase, staying below 27.5 kPa. The addition of the helmet changes this dynamic along with the waveform change shown in Fig. 11b. The rise to peak pressure on the lower back of the head (sensor 12) is abnormal but then decays normally, possibly due to the angled neck of the manikin. This angled neck changes the angle of incidence at which the shock wave impacts the back of the head, affecting the amount of force delivered to the head upon impact. In this orientation, when a helmet was added, the head overall expe-

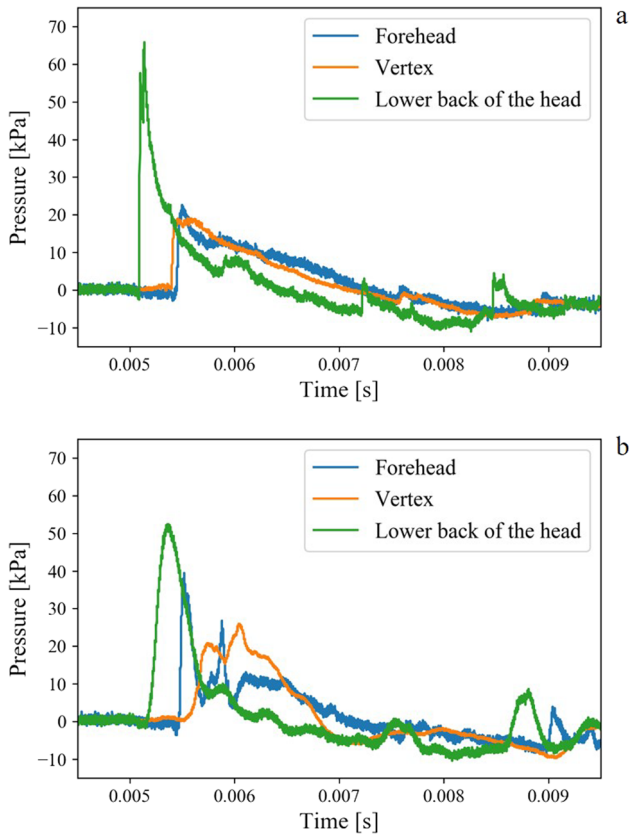

Fig. 10 **a** The 135-degree waveforms of the forehead, vertex, and lower back of the head sensors when not wearing a helmet. **b** The same sensors but with the addition of the helmet

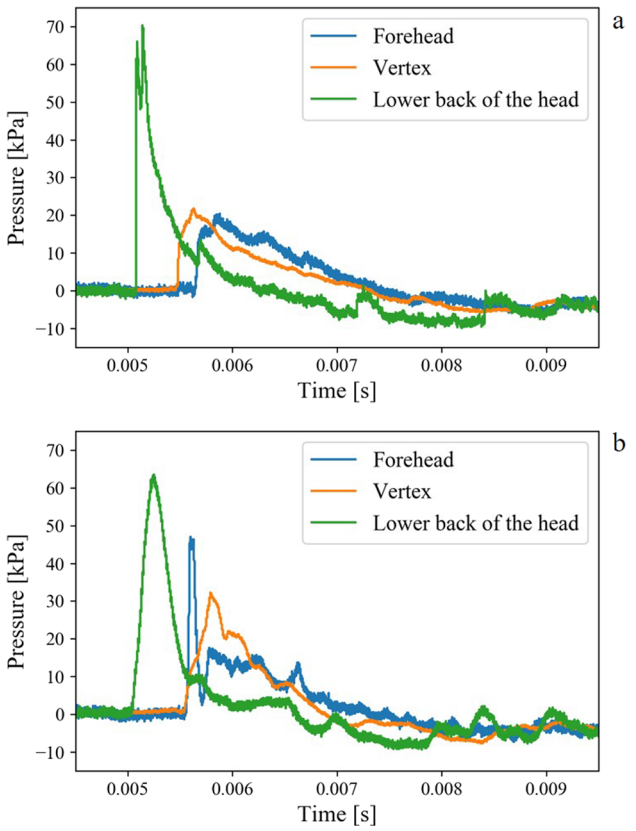

Fig. 11 **a** The 180-degree waveforms of the forehead, vertex, and lower back of the head sensors when not wearing a helmet. **b** The same sensors but with the addition of the helmet

rienced a 51% increase in peak overpressure, 28% increase in rise time, 5% increase in duration on the head, and 10% increase in impulse.

While wearing a helmet, the user experiences the highest average peak overpressure of 56.7 kPa on the head in the 180-degree orientation and the highest impulse of 20.8 kPa·ms when in the 0-degree orientation. However, the 90-degree orientation had the lowest average impulse of 16.4 kPa·ms and the second lowest average peak overpressure of 42.6 kPa. The 45-degree orientation had the lowest overall peak overpressure of 40.4 kPa, but the second highest impulse of 19.2 kPa·ms. These data are shown in Table 3 and were determined by averaging peak overpressure for sensors on the forehead, vertex, back the head, and both sides of the head (sensors 3, 6, 12, 14, and 15). These sensors were selected to present overall peak overpressure data from each side of the head. Earlier shock wave flow comparisons focused solely on sensors 3, 6, and 12 for clarity in figures. Compared to the 0-degree orientation while wearing a helmet, the 90-degree orientation resulted in the biggest reduction in overall peak overpressure of 8%, while the 180-degree orientation led to an increase by 29%. For impulse, the greatest reduction of 21% was seen in the 90-degree orientation, and the 0-degree orientation had the highest overall impulse of any orientation. In both cases of 0-degree and 180-degree orientations, the torso was parallel to the blast, which allowed the shock wave to reflect off the shoulders, part of the upper chest, and upper back into the helmet. For the 90-degree, only one shoulder faced the blast, thus reducing the surfaces for the wave to reflect off.

Table 3 indicates that the 0- and 180-degree orientations could result in higher injury compared to the other orientations tested based on the increased peak overpressure and impulse. This consolidation of values when the helmet is worn in Table 3 would mimic a battlefield scenario where a helmet must be worn. There are shock tube, free-field, and computational model studies in published literature supporting the notion that the 0-degree orientation is the most dangerous orientation in which the underwash effect under the helmet was observed [16, 23, 28]. Alternatively, a computational model study suggested that the 180-degree orientation could be the worst [35]. The results collected here are not in agreement with another study which observed that the highest overpressures were experienced in the 45-degree orientation [15]. In addition, the same study observed that the peak pressure is reduced the greatest in rear-facing trials with the rear of the head sensor [15]. The precise influence of orientation toward a blast is still under debate, but the

Table 3 Overall peak overpressures and impulses of each orientation when wearing a helmet

Orientation (degrees)	0	45	90	135	180
Overall peak overpressure (kPa)	44.1	40.4	42.6	46.8	56.7
Overall impulse (kPa·ms)	20.8	19.2	16.4	17.8	18.3

Table 4 Time duration for the blast wave to travel through and over the helmet recorded by high speed imaging

Orientation (degrees)	0	45	90	135	180
Time to travel under the helmet (ms)	0.61	0.58	0.73	0.75	0.64
Time to travel over the helmet (ms)	0.66	0.58	0.67	0.67	0.65

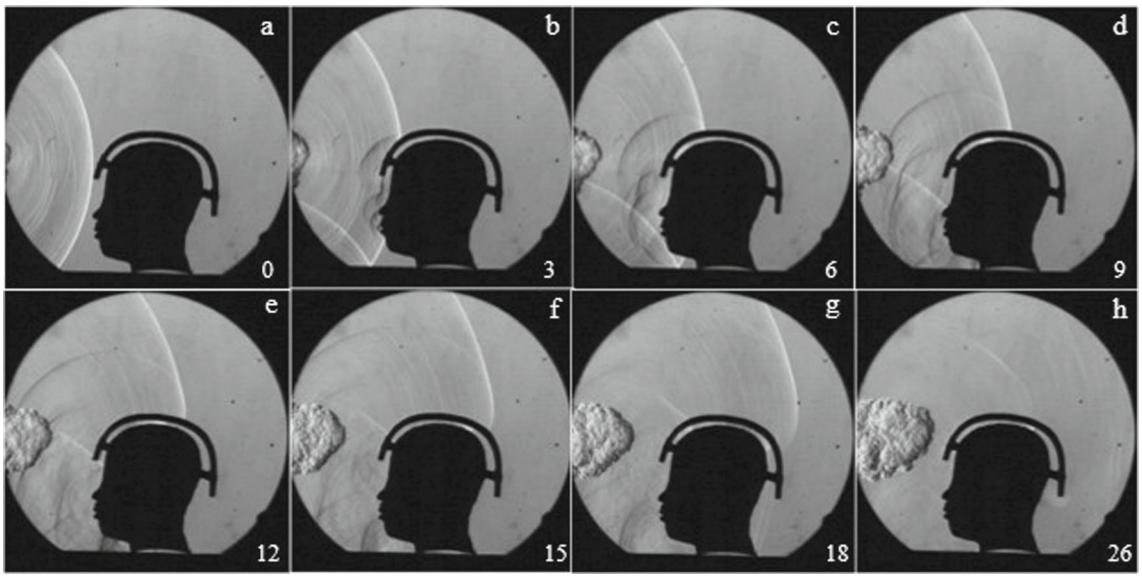

Fig. 12 Images (**a**) through (**h**): slow motion footage of shock wave progression over and under the helmet for a cross section of a warfighter wearing a helmet. Images start at the frame before interaction with the cross section (frame 0)

directionality toward the blast has been shown to make a significant difference, and the use of the helmet alters the shock loading on the head.

Shock wave flow was examined in each orientation using high-speed footage. The shock wave quickly impacted the head and exited out of the back of the helmet, creating an observable ejection. This allowed the duration of the wave's movement under the helmet to be measured. For 0-degree and 180-degree orientations, the wave took slightly longer to travel over the helmet than through it. Turning the manikin resulted in the wave traveling faster over the helmet, as seen from the data for the 90- and 135-degree orientations. The time to travel through the helmet is compared to the time to travel over the helmet in Table 4.

3.2 Schlieren imagery

Varying densities in gases caused by differences in temperature or high-speed flow create disturbances that refract light, and these disturbances can be visualized because of this refracted light [50]. Shock waves can induce these gas disturbances, enabling visualization of their propagation through such methods as shadowgraphy or schlieren. Here schlieren imaging helped see cross sections of shock wave flow under the helmet, an aspect of the underwash effect. In a 0-degree, front blast, the front of the head would receive head-on overpressure from the direct impact of the shock wave and cause reflections between the forehead and the helmet, as shown in Fig. 12a, b. However, the rest of the head would experience the overpressure caused by one or more obliquely reflected waves. The chin area may also be subjected to the overpressure associated with the Mach stem that is seen forming in Fig. 12c, along with smaller reflected waves trailing behind. After the wave has finished traveling over the head, this blast wave ejects out of the helmet cavity shown in Fig. 12h and observed in the free-field tests. Results from the free-field blasts showed how low-pressure waveforms could change as orientation changes with and without the helmet. These results can be combined with schlieren imaging to help explain why wave–helmet interactions resulted in non-traditional waveforms.

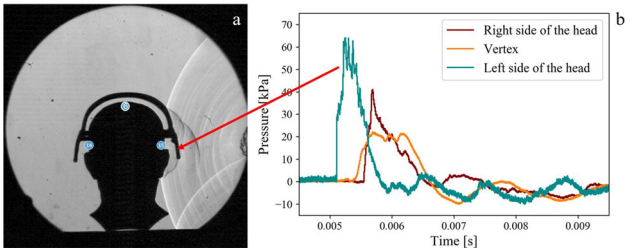

Fig. 13 **a** 90-degree schlieren interaction compared to the waveform of 90-degree free-field blast (**b**), from sensors 6, 14, and 15. Sensor numbers were placed over the image of the schlieren to show positions of where the sensors would be on the manikin used in free-field tests. Sensor 15 is the sensor closest to the free-field blast

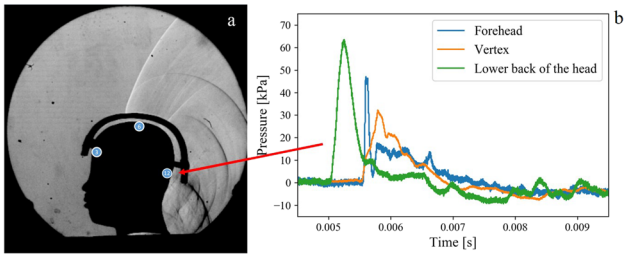

Fig. 14 **a** 180-degree schlieren interaction compared to the waveform of 180-degree free-field blast (**b**), from the forehead, vertex, and lower back of the head sensors. Sensor numbers were placed over the image of the schlieren to show positions of where the sensors would be on the manikin used in free-field tests

During a 90-degree blast, the shock wave propagated under the helmet from the side of the head sensor closest to the blast (sensor 15) to the vertex of the head (sensor 6, top of the head) and then to the sensor on other side of the head (sensor 14). The free-field blast data for the left, vertex, and right side of the head are shown in Fig. 13b. A visual representation of the schlieren data can be seen in Fig. 13a. The shock waves are shown to reflect between the side of the head and helmet, causing the time the shock wave is travelling through the helmet cavity to increase. This change in wave progression throughout the helmet led to high overpressures being maintained on the side of the head closest to the blast. This change in waveform indicates that the geometry of the helmet is an important design element, and surfaces under the helmet can cause continuous reflections in a specific area. When testing a helmet with the face protection of a mandible, Mott et al. noted the role geometry played when a shock wave was confined under the helmet at a particular area. In that case, a shock wave reflection off the shoulder propagated into the helmet cavity was trapped between the mandible and the face and created an area of high overpressure [27]. A solution is to allow the shock wave to escape quickly once inside the helmet to prevent areas of high overpressure, or another approach could be used to develop a method to dissipate the shock wave energy under the helmet.

A comparison of the data from the 180-degree free-field blast while the helmet was worn, to the schlieren experiment of the same angle is shown in Fig. 14b. The frame in Fig. 14a shows an area in which the shock wave is momentarily confined while repeatedly reflecting between the helmet and the head. This area is formed due to the downward geometry of the back of the head and the back of the helmet, preventing the wave from progressing away from the head. This area slows down the movement of the shock wave traveling under the helmet which increases overpressure by 10% compared to how the blast wave travels over the head during a 0-degree front blast. Wave propagation time on the back of the head is 11% longer due the presence of the helmet. The stem that forms as the shock waves interact and move under the helmet creates an area of high overpressure at the forehead sensor; however, that area of high overpressure has a short duration with the presence of the helmet, resulting in an increase in duration of only 5%. Allowing the helmet designers to understand which geometric features of a helmet shape aid in the propagation of a blast wave as the wave progresses is paramount for future helmet designs. From this analysis, curving the back of the helmet to allow the wave to reflect away from the head or allow the shock wave to quickly propagate outward would improve blast wave exposure times and levels. That being said, other methods could be developed to reduce the shock wave energy while it is under the helmet.

In this experiment, helmet pads were used in the free-field testing but were not represented in the 2D schlieren testing. The simplification of removing the pads in 2D schlieren testing allowed the shock wave motion through the helmet cavity to be easily visualized. Adding the helmet pads would have prevented observation of this motion in a 2D setting, but in contrast, in a 3D setting, the helmet pads do not entirely surround the head, with gaps between them. These gaps still allow shock wave motion, just not along a simple 2D path, as shown in schlieren tests. Further, pad–helmet–head shock reflections resulted in increasing the pressure of the air in that area. These increased pressures were seen in the free-field experiments conducted.

4 Conclusions

In this study, free-field and schlieren imagery tests from multiple orientations were conducted and compared for scenarios where a helmet was and was not worn. The underwash effect, in which high overpressure regions are created due to collisions under a helmet, was observed. From these combinations of tests, the lessons learned are: (1) With the addition of the helmet, the shock wave waveform is changed due to multiple reflections between the head and the helmet; recording simply the peak overpressure does not give the full story of how the waves affect the head. (2) When a helmet is worn, ori-

entation allows different parts of the head to be exposed and reflections off the shoulders to enter underneath, increasing the shock loading on the head. (3) Orientation stance affects the overall overpressure and impulse imparted on the head. It is recommended that future investigations include a torso in the test design due to the impact it has on the waveform profiles.

0-degree and 180-degree were the orientations in which the highest overall overpressures and impulses were experienced due to the addition of a helmet. Compared to the 0-degree, while wearing a helmet, the 180-degree increased peak overpressure by 29%. This is in part due to the reflections off the shoulders and into the helmet, causing additional collisions under the helmet. Wearing a helmet in the 90-degree and 45-degree orientations had the lowest overall overpressure, but the 90-degree one had an overall slight decrease in impulse. Compared to the 0-degree orientation while wearing a helmet, the 90-degree orientation resulted in the biggest reduction in overall peak overpressure of 8% compared to not wearing a helmet, and for impulse, the greatest reduction of 21%. The 90-degree and 45-degree orientations were not perpendicular to the blast, reducing reflections off the shoulders entering underneath the helmet. Both directions shielded a substantial amount of the head from a direct impact from the initial shock wave.

Those designing helmets may consider ways to shape the propagation of shock waves by understanding waves' propagation and reflections under and around the helmet to prevent increases in peak overpressure and impulse that would result in more skull flexure. Research into impedance mismatch of the materials and shock loading reduction used in helmet design is warranted and could reduce the effects discussed in this manuscript.

Supplementary Information The online version contains supplementary material available at https://doi.org/10.1007/s00193-024-01167-4.

Acknowledgements This research was supported by the Johnson Research Team, namely Martin Langenderfer, Kelly Williams, Emily Johnson, Everett Baker, Frank Schott, and Rachel Bauer aided during the schlieren and free-field tests.

Funding The authors did not receive support from any organization for the submitted work. There is no affiliation either direct or indirect between the authors and the sensor manufacturers referenced in this document.

Declarations

Conflict of interest The authors declare that they have no conflict of interest.

References

1. Kamimori, G.H., Reilly, L.A., LaValle, C.R., Olaghere Da Silva, U.B.: Occupational overpressure exposure of breachers and military personnel. Shock Waves 27(6), 837–847 (2017). https://doi.org/10.1007/s00193-017-0738-4
2. Belding, J.N., Egnoto, M., Englert, R.M., Fitzmaurice, S., Thomsen, C.J.: Getting on the same page: consolidating terminology to facilitate cross-disciplinary health-related blast research. Front. Neurol. **12**, 695496 (2021). https://doi.org/10.3389/fneur.2021.695496
3. Department of the Army Pamphlet 385-64, Safety Ammunition and Explosives Safety Standards. https://armypubs.army.mil/epubs/DR_pubs/DR_a/ARN31050-PAM_385-64-000-WEB-1.pdf (2011)
4. Rutter, B., Song, H., DePalma, R.G., Hubler, G., Cui, J., Gu, Z., Johnson, C.E.: Shock wave physics as related to primary non-impact blast-induced traumatic brain injury. Military Med. 186(Supplement_1), 601–609 (2021). https://doi.org/10.1093/milmed/usaa290
5. Kamnaksh, A., Kwon, S.-K., Kovesdi, E., Ahmed, F., Barry, E.S., Grunberg, N.E., Long, J., Agoston, D.: Neurobehavioral, cellular, and molecular consequences of single and multiple mild blast exposure: proteomics and 2DE. Electrophoresis **33**(24), 3680–3692 (2012). https://doi.org/10.1002/elps.201200319
6. Tate, C.M., Wang, K.K.W., Eonta, S., Zhang, Y., Carr, W., Tortella, F.C., Hayes, R.L., Kamimori, G.H.: Serum brain biomarker level, neurocognitive performance, and self-reported symptom changes in soldiers repeatedly exposed to low-level blast: a breacher pilot study. J. Neurotrauma **30**(19), 1620–1630 (2013). https://doi.org/10.1089/neu.2012.2683
7. Tham, C.Y., Tan, V.B.C., Lee, H.P.: Ballistic impact of a KEVLAR®helmet: experiment and simulations. Int. J. Impact Eng **35**(5), 304–318 (2008). https://doi.org/10.1016/j.ijimpeng.2007.03.008
8. Sone, J.Y., Kondziolka, D., Huang, J.H., Samadani, U.: Helmet efficacy against concussion and traumatic brain injury: a review. J. Neurosurg. **126**(3), 768–781 (2017). https://doi.org/10.3171/2016.2.JNS151972
9. Op't Eynde, J., Yu, A.W., Eckersley, C.P., Bass, C.R.: Primary blast wave protection in combat helmet design: a historical comparison between present day and World War I. PLOS ONE **15**(2), 0228802 (2020). https://doi.org/10.1371/journal.pone.0228802
10. Ouellet, S., Philippens, M.: The multi-modal responses of a physical head model subjected to various blast exposure conditions. Shock Waves **28**(1), 19–36 (2018). https://doi.org/10.1007/s00193-017-0771-3
11. Gupta, R.K., Przekwas, A.: Mathematical models of blast-induced TBI: current status, challenges, and prospects. Front. Neurol. **4**, 59 (2013). https://doi.org/10.3389/fneur.2013.00059
12. Fry, F.J., Barger, J.E.: Acoustical properties of the human skull. J. Acoust. Soc. Am. **63**(5), 1576–1590 (1978). https://doi.org/10.1121/1.381852
13. Cooper, P.: Explosives Engineering, p. 420. Wiley-VCH, New York (1997)
14. Baird, J.: Explosive shocks and impedance mismatch in armatures. Electromagn. Phenomena **3**(3), 405–413 (2003)
15. Mott, D.R., Schwer, D.A., Young, T.R., Levine, J., Dionne, J.-P., Makris, A., Hubler, G.: Blast-induced pressure fields beneath a military helmet (2008). Abstract ID: BAPS.2008.DFD.MF.8
16. Li, J., Ma, T., Huang, C., Huang, X., Kang, Y., Long, Z., Liu, M.: Protective mechanism of helmet under far-field shock wave. Int. J. Impact Eng. **143**, 103617 (2020). https://doi.org/10.1016/j.ijimpeng.2020.103617
17. Azar, A., Bhagavathula, K.B., Hogan, J., Ouellet, S., Satapathy, S., Dennison, C.R.: Protective headgear attenuates forces on the inner table and pressure in the brain parenchyma during blast and impact: an experimental study using a simulant-based surrogate model of the human head. J. Biomech. Eng. **142**(4), 041009 (2020). https://doi.org/10.1115/1.4044926

18. Downes, D., Bouamoul, A., Ouellet, S., Nejad Ensan, M.: Development and validation of a biofidelic head form model to assess blast-induced traumatic brain injury. J. Defense Model. Simul. Appl. Methodol. Technol. **15**(3), 257–267 (2018). https://doi.org/10.1177/1548512917737634
19. Chandra, N., Sundaramurthy, A., Gupta, R.K.: Validation of laboratory animal and surrogate human models in primary blast injury studies. Mil. Med. **182**(S1), 105–113 (2017). https://doi.org/10.7205/MILMED-D-16-00144
20. Ganpule, S., Gu, L., Alai, A., Chandra, N.: Role of helmet in the mechanics of shock wave propagation under blast loading conditions. Comput. Methods Biomech. Biomed. Eng. **15**(11), 1233–1244 (2012). https://doi.org/10.1080/10255842.2011.597353
21. Kumar, R.A., Pathak, V.: Shock wave mitigation using zig-zag structures and cylindrical obstructions. Defence Technol. **17**(6), 1840–1851 (2021). https://doi.org/10.1016/j.dt.2020.10.001
22. Haris, A., Lee, H.P., Tan, V.B.C.: An experimental study on shock wave mitigation capability of polyurea and shear thickening fluid based suspension pads. Defence Technol. **14**(1), 12–18 (2018). https://doi.org/10.1016/j.dt.2017.08.004
23. Skotak, M., Salib, J., Misistia, A., Cardenas, A., Alay, E., Chandra, N., Kamimori, G.H.: Factors contributing to increased blast overpressure inside modern ballistic helmets. Appl. Sci. **10**(20), 7193 (2020). https://doi.org/10.3390/app10207193
24. Karimi, A., Razaghi, R., Girkin, C.A., Downs, J.C.: Ocular biomechanics during improvised explosive device blast: a computational study using eye-specific models. Injury **53**(4), 1401–1415 (2022). https://doi.org/10.1016/j.injury.2022.02.008
25. Ganpule, S., Salzar, R., Perry, B., Chandra, N.: Role of helmets in blast mitigation: insights from experiments on PMHS surrogate. Int. J. Exp. Comput. Biomech. **4**(1), 13–31 (2016). https://doi.org/10.1504/IJECB.2016.10002680
26. Hosseini-Farid, M., Amiri-Tehrani-Zadeh, M., Ramzanpour, M., Ziejewski, M., Karami, G.: The strain rates in the brain, brainstem, dura, and skull under dynamic loadings. Math. Comput. Appl. **25**(2), 21 (2020). https://doi.org/10.3390/mca25020021
27. Mott, D.R., Young, T.R., Schwer, D.A.: Blast loading on the head under a military helmet: effect of face shield and mandible protection. 52nd Aerospace Sciences Meeting, National Harbor, MD, AIAA Paper 2014-0948 (2014). https://doi.org/10.2514/6.2014-0948
28. Zhang, L., Makwana, R., Sharma, S.: Brain response to primary blast wave using validated finite element models of human head and advanced combat helmet. Front. Neurol. **4**, 88 (2013). https://doi.org/10.3389/fneur.2013.00088
29. Tan, L.B., Chew, F.S., Tse, K.M., Chye Tan, V.B., Lee, H.P.: Impact of complex blast waves on the human head: a computational study: complex blast waves on the human head. Int. J. Numer. Methods Biomed. Eng. **30**(12), 1476–1505 (2014). https://doi.org/10.1002/cnm.2668
30. Zhang, T.G., Satapathy, S.S., Dagro, A.M., McKee, P.J.: Numerical study of head/helmet interaction due to blast loading. ASME 2013 International Mechanical Engineering Congress and Exposition, San Diego, CA, USA, Volume 3A: Biomedical and Biotechnology Engineering, Paper No: IMECE2013-63015, V03AT03A004 (2013). https://doi.org/10.1115/IMECE2013-63015
31. Jazi, M.S., Rezaei, A., Karami, G., Azarmi, F.: Biomechanical parameters of the brain under blast loads with and without helmets. Int. J. Exp. Comput. Biomech. **2**(3), 223 (2014). https://doi.org/10.1504/IJECB.2014.060400
32. Sarvghad-Moghaddam, H., Rezaei, A., Ziejewski, M., Karami, G.: CFD modeling of the underwash effect of military helmets as a possible mechanism for blast-induced traumatic brain injury. Comput. Methods Biomech. Biomed. Eng. **20**(1), 16–26 (2017). https://doi.org/10.1080/10255842.2016.1193597
33. Sarvghad-Moghaddam, H., Rezaei, A., Ziejewski, M., Karami, G.: Evaluation of brain tissue responses because of the underwash overpressure of helmet and faceshield under blast loading. Int. J. Numer. Methods Biomed. Eng. **30**(e02782), 22–2016 (2016). https://doi.org/10.1002/cnm.2782
34. Singh, D., Cronin, D.S.: Efficacy of visor and helmet for blast protection assessed using a computational head model. Shock Waves **27**(6), 905–918 (2017). https://doi.org/10.1007/s00193-017-0732-x
35. Sarvghad-Moghaddam, H., Jazi, M.S., Rezaei, A., Karami, G., Ziejewski, M.: Examination of the protective roles of helmet/faceshield and directionality for human head under blast waves. Comput. Methods Biomech. Biomed. Eng. **18**(16), 1846–1855 (2015). https://doi.org/10.1080/10255842.2014.977878
36. Sharma, M.R.Z.L. S.: Evaluation of blast mitigation capability of advanced combat helmet by finite element modeling. Dearborn, MI, USA (2012)
37. Grujicic, M., Bell, W.C., Pandurangan, B., Glomski, P.S.: Fluid/structure interaction computational investigation of blast-wave mitigation efficacy of the advanced combat helmet. J. Mater. Eng. Perform. **20**(6), 877–893 (2011). https://doi.org/10.1007/s11665-010-9724-z
38. Makris, A., Cheng, M., Dionne, J.-P., Levine, J.: EOD Helmet protection in small blast scenarios. Counter IED Report (2021). https://counteriedreport.com/eod-helmet-protection-in-small-blast-scenarios/
39. Tan, X.G., Bagchi, A.: Computational modeling of combat helmet performance analysis integrating blunt and blast loadings. ASME 2020 International Mechanical Engineering Congress and Exposition, Virtual, Online, Paper No: IMECE2020-23925, V005T05A052 (2020). https://doi.org/10.1115/IMECE2020-23925
40. Yu, X., Ghajari, M.: Protective performance of helmets and goggles in mitigating brain biomechanical response to primary blast exposure. Ann. Biomed. Eng. **50**(11), 1579–1595 (2022). https://doi.org/10.1007/s10439-022-02936-x
41. Mall, M.: Short realistic male bendable arms mannequin MM-BC8S. https://mannequinmall.com/products/short-realistic-male-bendable-arms-mannequin-mm-bc8s
42. PCB Piezotronics—Model 102B18. 3425 Walden Avenue Depew, NY 14043. https://www.pcb.com/products?m=102B18
43. Hi-Techniques—Synergy P | High Speed Data Acquisition. https://hi-techniques.com/products/synergy/p.html
44. Clear Ballistics. https://www.clearballistics.com/shop/10-ballistic-gelatin-fbi-block/
45. UFC 3-340-02, Structures to Resist the Effects of Accidental Explosions, 1943 (2005). https://www.wbdg.org/FFC/DOD/UFC/ARCHIVES/ufc_3_340_02.pdf
46. Swisdak, M.M.: Explosion Effects and Properties. Part I. Explosion Effects in Air. Technical report, Naval Surface Weapons Center White Oak Lab (1975). https://apps.dtic.mil/sti/citations/ADA018544
47. Phantom v2012. https://www.phantomhighspeed.com/-/media/project/ametekxa/visionresearch/documents/datasheets/web/wdsuhsfam.pdf?download=1

48. NONEL lead line technical data sheet. Dyno Nobel. https://www.dynonobel.com/resource-hub/products/nonel-lead-line
49. Du, Z., Li, Z., Wang, P., Wang, X., Zhang, J., Zhuang, Z., Liu, Z.: Revealing the effect of skull deformation on intracranial pressure variation during the direct interaction between blast wave and surrogate head. Ann. Biomed. Eng. **50**(9), 1038–1052 (2022). https://doi.org/10.1007/s10439-022-02982-5
50. Settles, G.S.: Schlieren and Shadowgraph Techniques Visualizing Phenomena in Transparent Media, p. 26. Springer, Berlin (2001)